Article

Internal Characteristics of Air-Supplied Plasma Synthetic Jet Actuator

Rubing Liu [1,2,*], Shenghui Xue [1,2], Wentao Wei [1,3], Qi Lin [1,2] and Kun Tang [4,5]

1 School of Aerospace Engineering, Xiamen University, Xiamen 361102, China
2 Fujian Province Key Laboratory of Plasma and Magnetic Resonance Research, Xiamen 361102, China
3 Chengdu Aircraft Design Institute, Chengdu 610041, China
4 Key Laboratory of Rotor Aerodynamics, China Aerodynamic Research and Development Center, Mianyang 621000, China
5 Science and Technology on Plasma Dynamics Laboratory, Air Force Engineering University, Xi'an 710038, China
* Correspondence: lrb@xmu.edu.cn

Abstract: Conventional plasma synthetic jet actuators rely only on jet orifice for suction when functioning for long durations. A limited supplementary gas leads to jet velocity reduction and weakening of the flow control ability. Therefore, this study proposes an air-supplied actuator with a check valve externally connected to the cavity to improve its gas-supplying ability and jet performance. A quartz glass discharge chamber is developed to clarify the internal working mechanism of the air-supplied actuator. High-speed schlieren is employed to photograph the internal flow field of the discharge chamber. The results reveal that the inhalation airflow velocity of the jet orifice is doubled when the actuator is continuously working in the effective frequency band under the combined action of additional air supply from the check valve in the inhalation recovery stage. The gas pressure in the cavity is closer to the initial discharge state, discharge breakdown voltage is higher, discharge energy is stronger, and the process of gas expansion to generate a jet is less affected by the core defect of the heat source, thereby significantly increasing the jet velocity and saturation operating frequency of the actuator. The obtained results have important implications for the performance optimization of the air-supplied actuator.

Keywords: plasma synthetic jet; air-supplied actuator; high-speed schlieren; secondary jet

1. Introduction

Synthetic jet is a kind of discontinuous jet generated due to the alternate blowing and sucking of the surrounding fluid by the actuator, which has the advantages of compact structure, light weight, and no additional gas source, and has received a lot of attention from many researchers [1]. The plasma synthetic jet actuator (PSJA) was first developed by Kenneth et al. [2–6] from the Applied Physics Laboratory at Johns Hopkins University (JHU-APL) in the United States. PSJA has broad application prospects in the field of active flow control owing to its rapid response speed, wide excitation frequency band, easy adjustment, simple and stable structure, and absence of moving parts. At present, relevant experimental studies have been conducted in low-subsonic [7–9] and supersonic wind tunnels [10–13]. Various flow control objects include wings [7], flying wings [8], nozzles [9], flat plates [10,12], oblique wedges [11,13], blunt bodies [12], and transport aircraft rear bodies [14].

The conventional PSJA consists of an insulating closed cavity with a jet hole, a cathode, and an anode (Figure 1). Its operating process includes three stages: energy deposition, jet ejection, and inspiratory recovery [2]. The spark discharge produces a large sum of heat, and the air in the cavity is heated and rapidly expands. The jet is formed from the hole, and the external gas is backfilled to prepare for the next discharge [15].
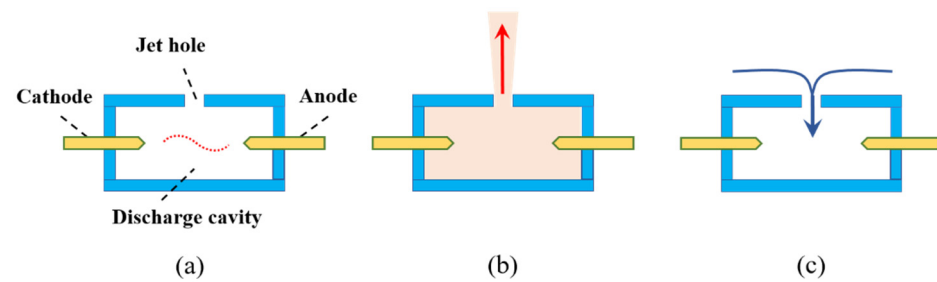
Figure 1. Operation process of plasma synthetic jet actuator (PSJA): (**a**) energy deposition; (**b**) jet ejection; (**c**) inspiratory recovery.

Studies on the PSJA have reported that the current structure of the actuator is insufficient. After the synthetic jet is ejected, the pressure in the actuator cavity depends only on the inspiratory recovery of the jet hole, and the supplementary gas is limited. As the actuator operating time increases, the cavity is heated, gas replenishment in the cavity is insufficient, jet velocity decreases, and flow control ability weakens [16–24].

To solve these problems, scholars have proposed various solutions. Zhou et al. [18] realized rapid replenishment and pressurization of the operating medium in the cavity by introducing high-speed incoming flow through the stamping inlet in a rarefied atmospheric environment. Their theoretical calculation and numerical simulation results revealed that the initial gas density of the cavity before the discharge of the stamping PSJA in the supersonic flow increased by 60%, and the average mass flow rate of the cavity backfill phase could be increased by approximately 85%. Li et al. [19] developed a novel actuator with a piezoelectric vibrator to improve inspiratory recovery; preliminary numerical simulation results revealed that the inspiratory recovery ability of the actuator is closely related to the amplitude of the piezoelectric vibrator, which can effectively improve the peak velocity of the jet. Emerick [10,20] and Zhou [21] used an external gas source to increase the velocity of the actuator. Zong et al. [22] and Zheng et al. [23] proposed a self-supplemented double-cavity PSJA by setting a subcavity below the main cavity for gas injection to increase the saturation frequency of the actuator.

Previously, we proposed an air-supplied PSJA [24]. This actuator does not require an additional high-pressure gas source and pipeline, nor does it rely on the flow pressure. It uses a one-way valve to improve the inspiratory recovery ability of the actuator, thereby improving jet performance. In the inspiratory recovery stage, the air-supplied actuator is supplemented by an external one-way valve and jet hole simultaneously, which can quickly fill the cavity after the jet is ejected, improve the discharge frequency of the actuator, and increase jet energy (Figure 2). Previous studies have investigated the performance enhancement effect of one-way valve on plasma synthetic jet (PSJ) actuator and illustrated the working mechanism of one-way valve to enhance the performance of actuator by measuring the energy deposition and internal pressure variation of the actuator [15]. However, the evolution of internal flow structure in the cavity has not been determined, especially the effect of air supply through one-way valve on the internal flow. The above research is an important guideline for the performance optimization of air-supplied PSJ.

Herein, to explore the internal flow mechanism of a one-way valve and improve the jet velocity characteristics, a quartz glass vapor injection actuator was designed, and high-speed schlieren technology was employed to photograph the internal flow of the discharge cavity during the operation of the air-supplied PSJA. The flow state of gas in the cavity at different operating stages was investigated when the actuator discharged. The internal flow mechanism of the jet velocity characteristics of the one-way valve air supplement was explored by comparing the differences in the gas flow inside the actuator under different states and operating frequencies, and an internal flow model was established to guide further optimization of the air-supplied PSJA.
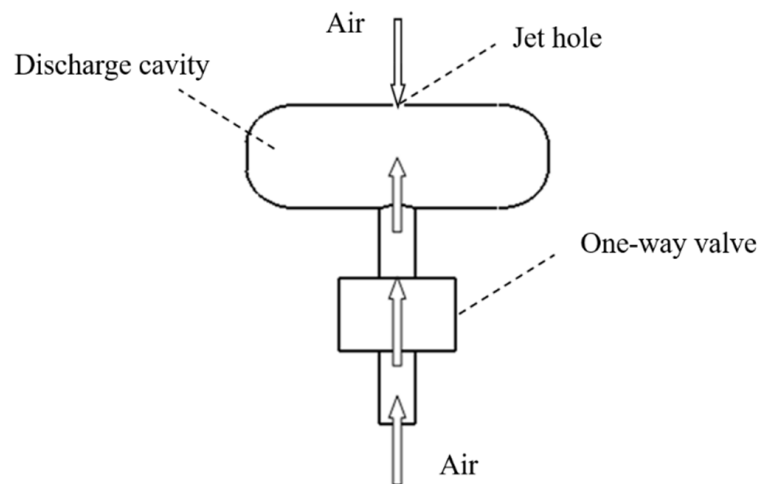
Figure 2. Scheme of air supplement via the one-way valve.

2. Experimental Setup

To study the discharge characteristics of the air-supplied PSJA and the flow characteristics in the discharge cavity, an experimental system was established for testing the internal flow field and discharge characteristics of the actuator cavity (Figure 3). The experimental setup primarily included a quartz vapor air-supplied PSJA, programmable high-voltage pulse power supply, discharge characteristic measurement system, and a high-speed schlieren measurement system.
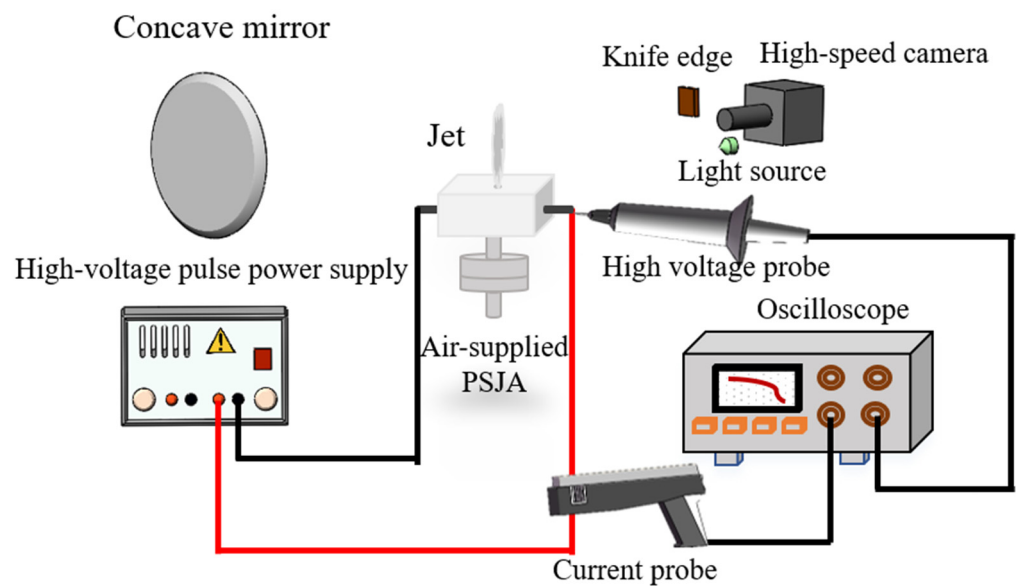
Figure 3. Schematic of the experimental setup.

### 2.1. Quartz Gas-Supplemented Plasma Synthetic Jet Actuator

PSJA cavity was studied using the experimental method proposed by Dong et al. [25], and a schlieren system was employed to photograph the internal flow of the actuator cavity. Therefore, a quartz-air-supplied PSJA was designed and fabricated. The actuator consisted of a quartz discharge cavity, air supplement one-way valve, anode, and cathode (Figure 4).
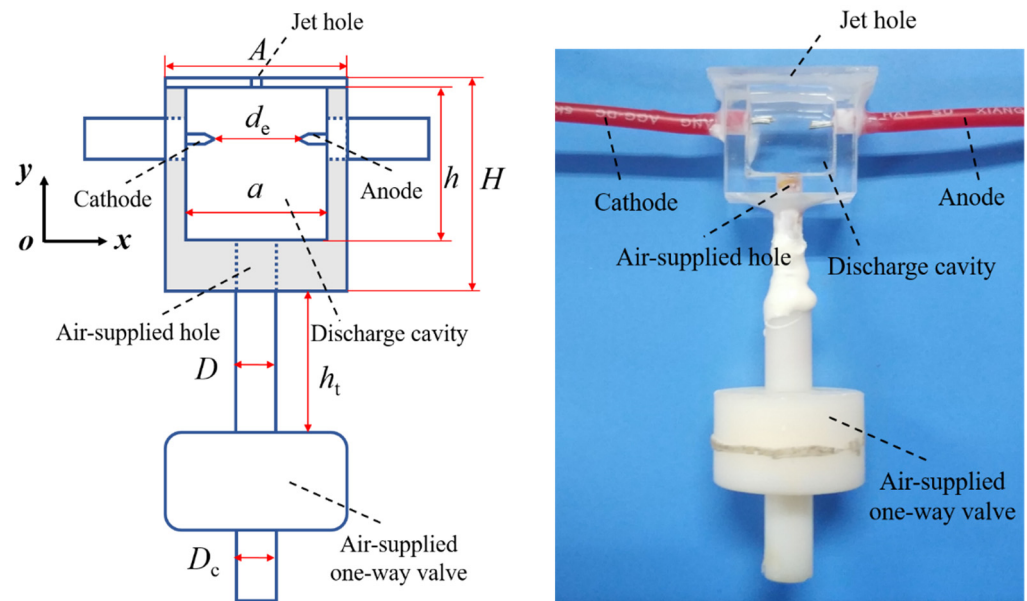
Figure 4. Structure of the air-supplement PSJA.

The quartz discharge cavity of the actuator was bonded with quartz glass of good light transmission performance, and the discharge cavity had a flat rectangular shape. The thickness of the light-transmitting side wall of the cavity was only 1 mm, which is convenient for the schlieren system to measure the gas flow state. The jet and filling holes were in the middle of the upper and lower sides of the discharge cavity, respectively. Electrodes of the actuator were located on the left and right sides of the discharge cavity.

The one-way air supply valve primarily comprises an inlet end, spool, and outlet end (Figure 5). It was found that the spool of the one-way valve was deformed and leaked air because the response speed of the silicone spool of the valve could not meet the required air supply frequency for the experiment [26]. Therefore, a special design of the one-way valve structure was carried out to enhance the air supply effect of the one-way valve. The valve core support structure inside the outlet end was designed as a conical boss, and a hole was made at the bottom of the boss to allow gas to enter and exit [27]. The conical boss has a buffering effect on the reverse airflow while supporting the spool, and the reverse airflow that originally directly impacts the spool acts on the inner surface of the conical cavity, effectively preventing the high-pressure airflow to strike the spool.
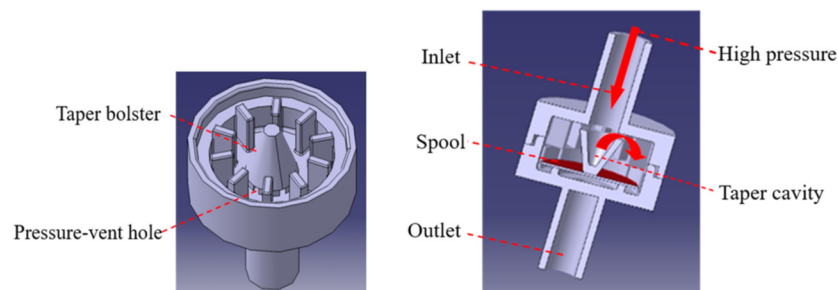
Figure 5. Structure of the one-way valve.

The outlet end of the one-way valve was connected to the air hole in the actuator cavity and fixed by a high-temperature-resistant silica sealing gel. Owing to the complex internal structure of the one-way valve, processing using the quartz material is difficult, and some structures (including the inlet and exhaust ends) have large curvatures and narrow gas pipelines. Hence, observing the internal gas flow state under the schlieren light path is

difficult. The detailed structural parameters of the quartz gas-supplemented actuator are presented in Table 1.

Table 1. Parameters of the quartz air-supplied plasma jet actuator.

Parameters	Value (mm)
Length A	18
Width B	7
Height H	20
Cavity length a	14
Cavity width b	5
Cavity height h	15
Electrode gap d_e	7
Jet hole height h_j	1
Jet hole diameter d	1
Outlet throat length h_t	30
Spool thickness h_s	0.4
Inlet diameter D_c	4
Air-supplied hole diameter D	4

2.2. Power Source and Discharge Characteristic Measurement Setup

The power source (XMU-PTLA-DY-02) can be controlled using a program, and its output voltage range is 0–20 kV, duty cycle is 5–50%, and frequency is 20–5 kHz.

The discharge characteristic measurement system of the actuator was established, and it primarily included an oscilloscope (Tektronix TBS2104), high-voltage probe (Tectronix P6015A), and current probe (Tectronix TCP0150). The discharge voltage and current changes of the vapor-injection actuator under different operating frequency bands and excitation states were measured.

2.3. High-Speed Schlieren Measurement System

A high-speed schlieren measurement system was used to study the flow evolution in the cavity of the air-supplied plasma synthetic jet actuator, and the measurement method was kept consistent with the literature [28]. The high-speed camera model was Photron FASTCAM SA-Z, the frame rate was set to 100,000 fps, the exposure time was 159 ns, and the image resolution was 640 × 280 pixels. The spatial resolution of the images was 0.28 mm/pixel, and the minimum image resolution was 0.5 pixels. The time interval between the two images was 10 μs. Therefore, the measurement error of the plasma synthetic jet front motion velocity was ±14 m/s, which corresponds to a distance of 0.5 pixel (0.14 mm) divided by 10 μs.

Ripple shadow images of the synthetic jet were taken for the entire process from generation to the end, then the position of the jet front in the images was identified, and from this the displacement of the jet front during a certain period of time was obtained, and finally the average velocity during that period of time was obtained using the velocity equation.

3. Characteristics Measurement Experiment of Air Supplement PSJA

According to previous studies [15], the effect of the one-way valve air supply on the PSJA is different at different frequencies, and it can be divided into effective and ineffective frequency bands. Therefore, herein, an excitation frequency in the f range of 60–300 Hz was selected for the experiment; the excitation voltage was U = 15 kV, excitation signal pulse width was t_p = 1 ms, and frequency interval was Δf = 20 Hz. In the experiment, the vapor-injection PSJA exhibited an air supplement excitation state and conventional excitation state. In the air supplement excitation state, the actuator can complete vapor injection via the bottom vapor injection hole through a one-way valve. In the conventional excitation state, the actuator is still externally connected with a one-way valve; however, the inlet end of the one-way valve is closed with silicone sealant to eliminate the vapor injection effect.

Without loss of generality, the typical operating frequencies f = 80 Hz (invalid frequency band) and f = 200 Hz (effective frequency band) were selected to measure the discharge characteristics and perform high-speed schlieren experiments. The discharge and flow performance of the PSJA under different excitation states were compared. The reasons for the difference in the air supply effect of the one-way valve under different excitation frequencies were analyzed, and the internal flow mechanism of the air-supplied PSJA was clarified.

3.1. Ineffective Frequency Band

3.1.1. Discharge Characteristic Measurement

When f = 80 Hz, the air-supplied actuator was in an invalid frequency band, and the air supplement excitation could not improve the discharge parameters of the actuator (Figure 6). In the conventional excitation state, the discharge peak voltage of the actuator was 11.3 kV and the peak current was 31.5 A. The peak voltage was 11.7 kV and peak current was 30 A under air supplement excitation. The peak voltage and current of the actuator discharge did not significantly change under the two excitation states.
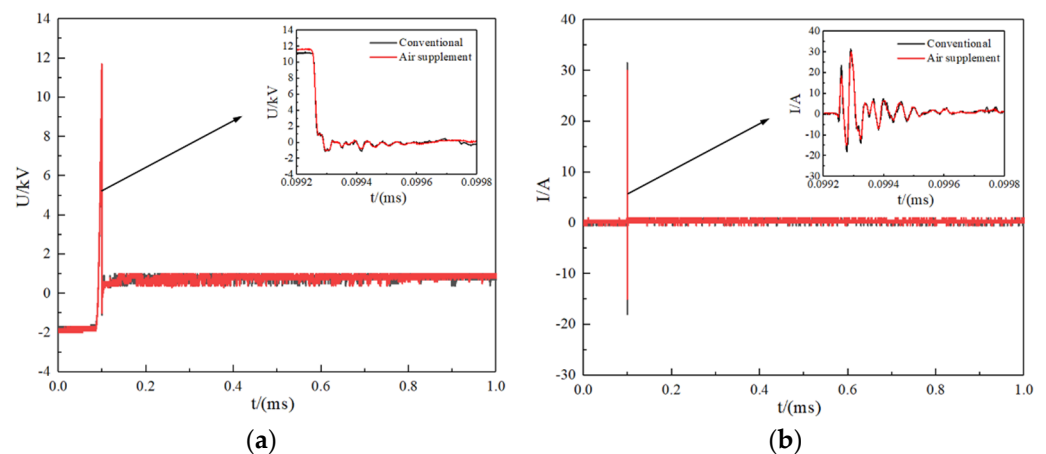

Figure 6. Voltage and current waveforms for different excitation states at f = 80 Hz: (**a**) voltage; (**b**) current.

3.1.2. Flow Field Evolution in Cavity

The typical operating frequency f = 80 Hz (invalid frequency band) was selected to photograph the working process of the actuator in continuous multiple discharge cycles in the air supplement excitation state and the conventional excitation state.

1. Air supplement excitation state

The flow field state in the cavity under the air supplement excitation state is shown in Figure 7. The instant air between the actuators was broken down by the high voltage, spark discharge occurrence was considered to be the starting time, that is, t = 0 μs. At t = 10 μs, the discharge spark was extinguished, and the gas density between the two electrodes changed because of the intense heating effect of the high-temperature plasma generated by the spark discharge, thus forming a clear strip-like core of the heat source. The heat source core continued to expand, and the pressure in the cavity raised rapidly, thereby forcing a part of the gas in the discharge cavity to eject outward via the jet hole. At t = 120 μs, a high-velocity jet was appeared at the jet orifice, and part of the gas was ejected into the one-way valve cavity via the lower air supply hole of the discharge cavity. At t = 1300 μs, the cavity no longer ejected gas and the jet ceased.
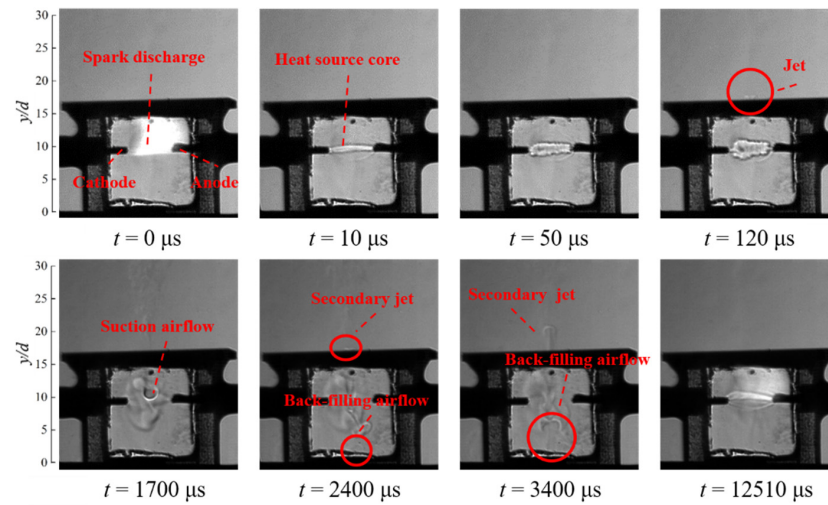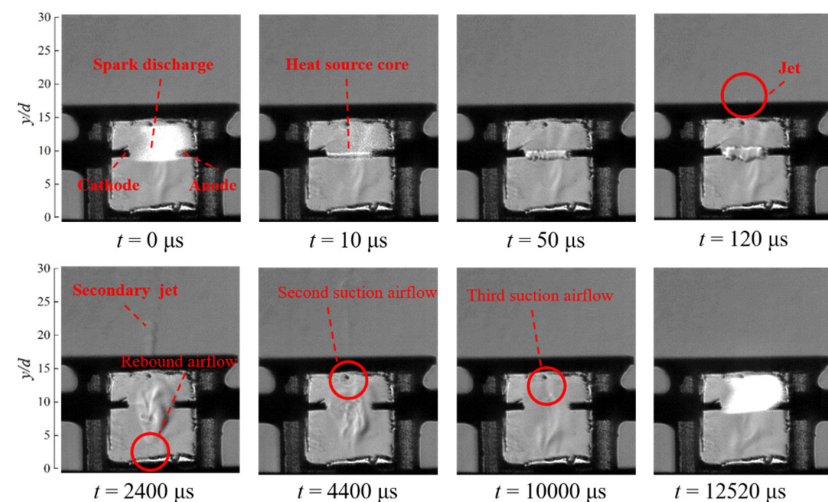
Figure 7. Evolution of the flow field in the cavity at f = 80 Hz under the air supplement excitation state.

After jet injection, the fluid entered the inspiratory recovery phase. The pressure in the discharge cavity was lower than the atmospheric pressure outside the cavity. Driven by internal and external pressure differences, the atmosphere outside the cavity was backfilled into the discharge cavity from the jet hole. At t = 1700 μs, the suction airflow front moved to the center of the discharge cavity.

At t = 2400 μs, the airflow moved upward from the discharge cavity position, which is the one-way valve-backfilling airflow. Simultaneously, a secondary jet appeared at the jet outlet of the actuator. The secondary jet velocity was extremely slow, and the jet height was limited. The jet was generated at t = 2400 μs and ceased at t = 5000 μs. From t = 10,000 μs onward, the gas in the discharge cavity returned to the state before discharge in preparation for the next discharge cycle.

2. Conventional excitation state

The flow-field state in the cavity under a conventional excitation state is shown in Figure 8. The discharge process and jet generation process were similar to those under the air supplement excitation state; however, at t = 1750 μs, a secondary jet appeared. Compared with the air supplement excitation state, the secondary jet appeared earlier and faster in the conventional excitation state.


Figure 8. Evolution of the flow field in the cavity at f = 80 Hz under conventional excitation.

At t = 2400 μs, the airflow moved upward from the position of the discharge cavity; this airflow was a one-way valve rebound airflow. In the conventional excitation state, because the one-way valve is in a closed state, the airflow was primarily from the jet occurring in the one-way valve cavity to form the gas owing to differential pressure rebound, perpendicular to the upward development of the air supply hole.

Subsequently, at t = 4400 and 10,000 μs, the second and third suction airflows were observed, respectively. In the conventional excitation state, the jet hole had three suctions and the three suction airflow velocities decreased. In addition, the intensity decreased, and the airflow was unclear during the third time. The above phenomenon of multiple inspiratory recoveries is a typical feature of conventional plasma synthetic jets [29].

3.　Comparative analysis

A comparison of the height and velocity of the jet front movement (Figure 9) revealed that the dimensionless height Hj/d of the jet front under the conventional excitation state was higher than that under the air supplement excitation state, and the peak velocity of the jet front movement was slightly higher. This indicates that the air-supplemented actuator is indeed in the invalid working frequency band; that is, the one-way valve does not play a role in improving the jet performance. This is consistent with previous research [15]. In the invalid working frequency band, the primary reason for the decrease in the jet peak velocity under the air supplement excitation state is that the peak pressure inside the discharge cavity exceeds the critical value of the reverse impact that the one-way valve spool can withstand at low frequencies, and the one-way valve has a reverse air leakage [15].
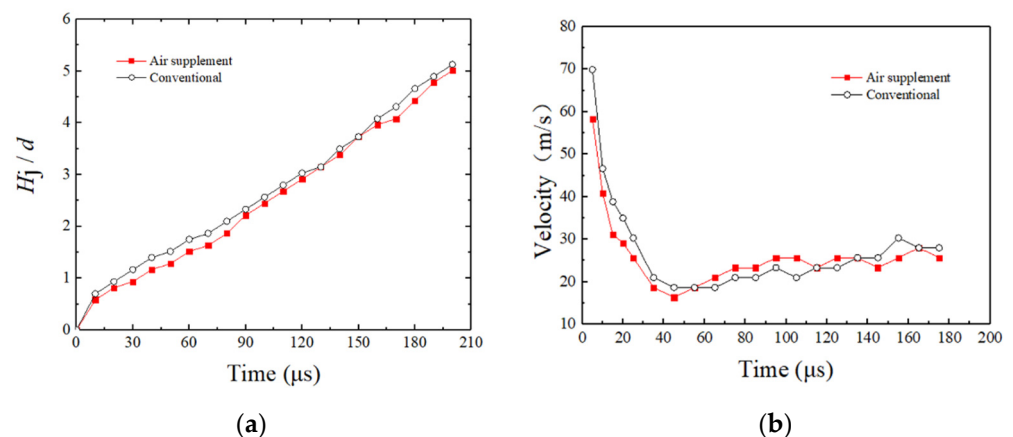
Figure 9. Curve of jet parameters with time at f = 80 Hz: (**a**) dimensionless height; (**b**) velocity.

A comparison of the two inspiratory airflows recovered by suction (Figure 10) revealed that compared with the conventional excitation state, the inspiratory airflow velocity of the actuator backfilled through the jet hole was higher, and the inspiratory airflow velocity of the actuator backfilled via the filling hole was lower. Because the pressure in the actuator cavity was lower and the pressure difference between the inside and outside was larger under the condition of air supplement excitation [15], the suction speed backfilling via the jet hole was higher. Simultaneously, owing to the leakage of the one-way valve in the air supplement excitation state, the pressure in the one-way valve cavity, internal and external pressure difference, and return airflow speed of the one-way valve decreased. However, because the backfilling air flow includes the initial rebound air flow of the one-way valve and the follow-up one-way valve, which continues to supply air from the outside, the duration of the backfilling air flow was much greater than that of the rebound air flow under the conventional excitation state. Therefore, only one inspiratory recovery is required to recover the actuator to the initial state in the air supplement excitation state, whereas three inspiratory recoveries are required to restore the initial state in the conventional excitation state.
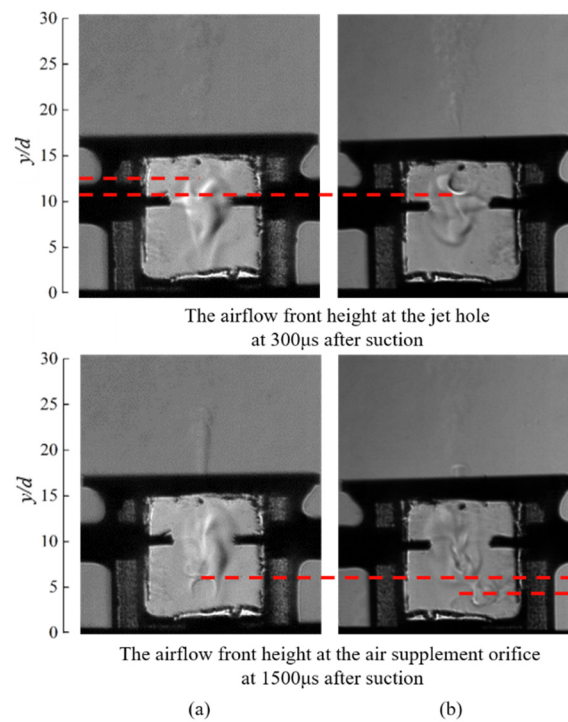
Figure 10. Comparison of inspiratory airflow front heights under two excitation states: (**a**) conventional excitation; (**b**) air supplement excitation.

3.2. Effective Frequency Band

3.2.1. Discharge Characteristic Measurement

When the gas-filled actuator is in the effective frequency band, air supplement excitation can increase the peak voltage and current of the actuator discharge. In the conventional excitation state, the discharge peak voltage of the actuator was 11.3 kV and peak current was 20 A (Figure 11). Whereas under supplement excitation, the peak voltage was 12.1 kV and peak current was 25.5 A. Thus, compared with the conventional excitation, the discharge peak voltage of the actuator increased by 0.8 kV, corresponding to a 7.1% increase, and the peak current increased by 5.5 A, corresponding to a 27.5% increase.
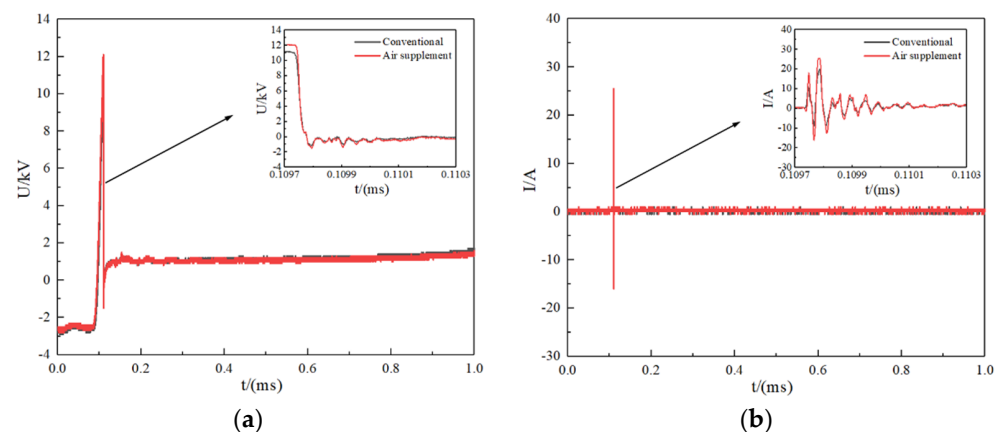
Figure 11. Voltage and current waveforms for different excitation states at f = 200 Hz: (**a**) voltage; (**b**) current.

The discharge energies for a single cycle of the actuator under each working condition were compared (Table 2). The discharge energy was obtained by integrating the product of the discharge voltage and current [15].

Table 2. Discharge energy of the actuator in a single cycle under different working conditions.

| Work Conditions		Discharge Energy (mJ)
Invalid frequency band	Conventional excitation	0.747
	Air supplement excitation	0.746
Effective frequency band	Conventional excitation	0.408
	Air supplement excitation	0.485

When f = 80 Hz, the single-cycle discharge energy was 0.747 and 0.746 mJ in the conventional and air supplement excitation states, respectively. Thus, the vapor injection of the one-way valve did not improve the single-cycle discharge energy of the actuator. When the energy conversion efficiency was constant, the energy used to generate the synthetic jet did not increase significantly. Finally, the dimensionless height of the jet front and the moving speed of the jet front under the air supplement excitation state were similar to those under the conventional excitation state (Figure 9).

When f = 200 Hz, the single-cycle discharge energy was 0.408 and 0.485 mJ in the conventional and air supplement excitation states, respectively, i.e., the discharge energy increased by 18.9%. As abovementioned, the energy used to generate the synthetic jet increased; consequently, the dimensionless height of the jet front was higher under the air supplement excitation state, the jet front moved faster, and the jet performance improved (Figure 11).

3.2.2. Flow Field Evolution in Cavity

1. Air supplement excitation state

The evolution of flow field in the cavity under the air supplement excitation state is shown in Figure 12. After the spark discharge, the heat source core expanded and a synthetic jet was generated and eventually ceased at t = 1300 μs. Concurrently, the internal and external pressure difference caused the discharge cavity to inhale and backfill, and inspiratory airflow was observed at the jet hole. At t = 4950 μs, inspiratory airflow could still be observed in the cavity, thus indicating that the inspiratory process of the jet hole continued until the next cycle before discharge, and the actuator began working in the next cycle with insufficient recovery.
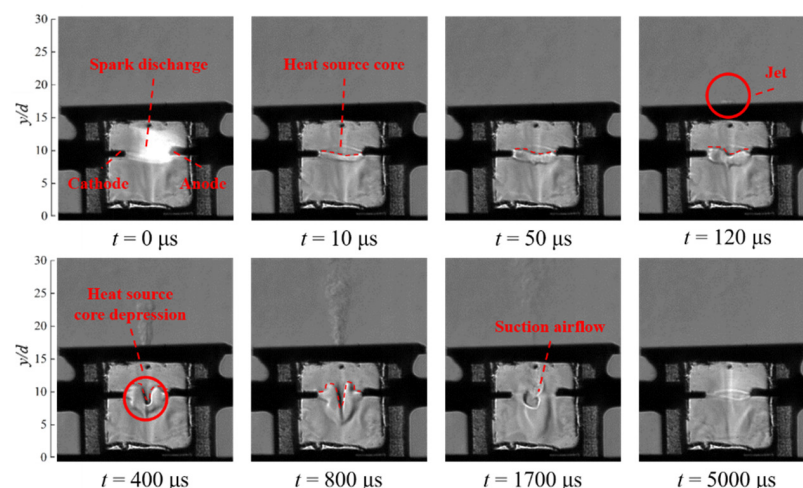
Figure 12. Evolution process of the flow field in the cavity at f = 200 Hz under the air supplement excitation state.

2. Conventional excitation state

The evolution of flow field in the cavity under conventional excitation is shown in Figure 13. After spark discharge and heat source core expansion, a synthetic jet was

generated and continued to develop until t = 1450 μs, and the pressure difference inside and outside the cavity caused the discharge cavity to begin inhaling. The upper part of the discharge cavity was aspirated through the jet hole, and the gas in the lower one-way valve rebounded to the discharge cavity through the makeup hole. At t = 2000 μs, these two streams of air flow moved toward each other, and a secondary jet appeared at the jet hole. At t = 2450 μs, the two airflows in the cavity met, and the rebound airflow intensity was higher. After the airflow was absorbed by the flushing jet hole, it continued to move upward and gradually diffused into the cavity, and the secondary jet continued to develop gradually.
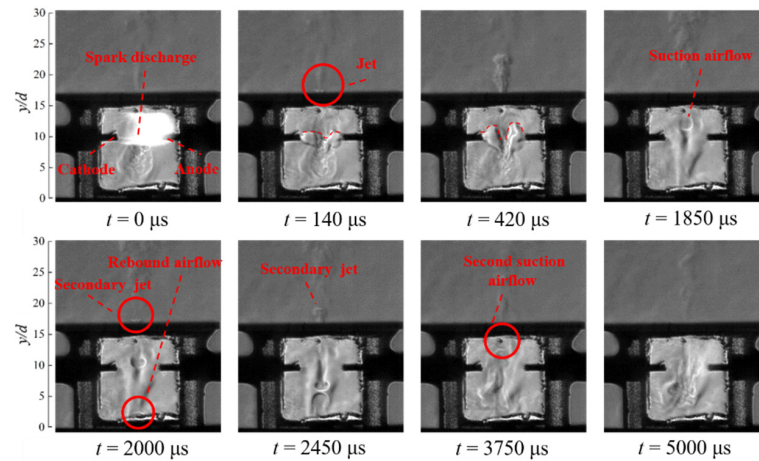

Figure 13. Evolution process of the flow field in the cavity at f = 200 Hz under conventional excitation.

At t = 3750 μs, the secondary hole at the jet hole absorbed air and continued to fill the air pressure in the discharge cavity. At t = 4950 μs, as revealed by the schlieren image, the flow field density in the cavity remained uneven and inspiratory airflow could be observed, thus indicating that the second inspiratory process of the jet hole continued until the discharge of the next cycle, and the actuator began operating in the next cycle with insufficient restoration.

3. Comparative analysis

A comparison of the moving height and speed of the jet front (Figure 14) revealed that the dimensionless height Hj/d of the jet front under air supplement excitation was higher than that under conventional excitation at the same time after jet generation, and the peak speed of the jet front movement was slightly higher. This suggests that the air replenishing actuator is indeed in the effective working frequency band, and the one-way valve plays a role in improving jet performance. This result is consistent with previous studies [15].
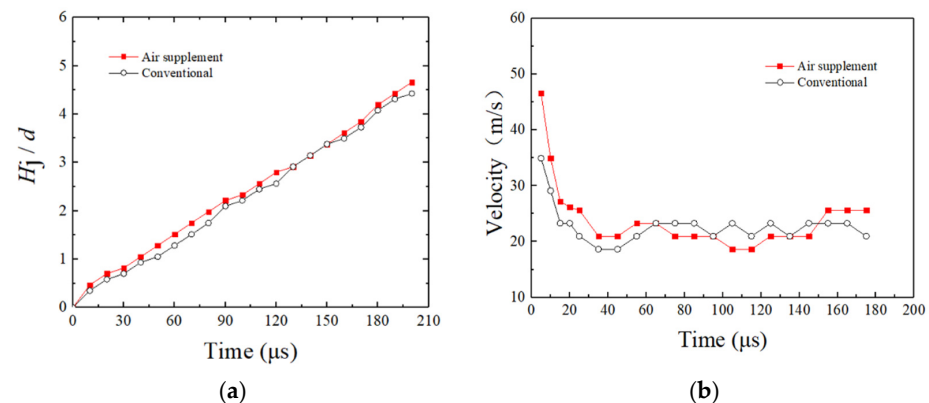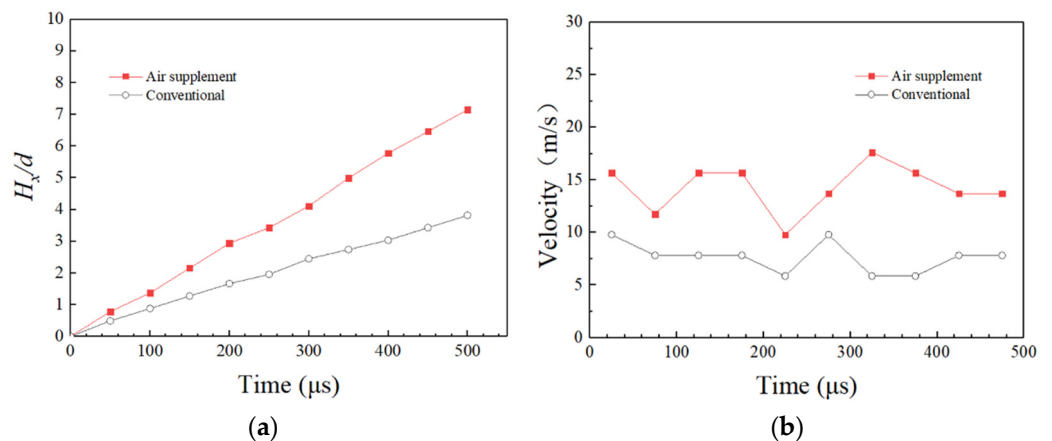

Figure 14. Curve of the jet parameters with time at f = 200 Hz: (**a**) dimensionless height; (**b**) velocity.

From the qualitative analysis of the ripple shadow image (Figure 15), after 300 μs of the suction, the airflow front height at the jet hole is higher in the air supplement excitation state compared with the conventional excitation state. Compared with the conventional excitation, the dimensionless height of the jet-hole suction airflow is significantly higher in the air supplement excitation state (Figure 16a), and the gap becomes more distinct. The overall velocity of the suction airflow is larger than that of the conventional excitation state, and at t = 320 μs, the speed of the suction airflow in the air supplement excitation state is nearly three times that of the conventional excitation state. This indicates that the pressure difference between the inside and outside of the actuator cavity is greater under the condition of air supplement excitation [15], which enables rapid air suction backfill through the jet orifice. In addition, a comparison of the inspiratory duration in the inspiratory recovery process revealed that the inspiratory duration of the actuator was only in the air makeup state once, whereas the inspiratory duration of the actuator in the conventional state required two or even three times to complete the inspiratory recovery process. This indicates that the inspiratory recovery effect can be improved by supplementing air via a one-way valve. When air is supplemented, the inspiratory recovery of the actuator is faster, and the gas state can be fully recovered to the initial state. This is helpful for the actuator to maintain a continuous and stable high-speed jet under the continuous high-frequency working state and can improve the saturated working frequency of the actuator to avoid premature 'misfire'.
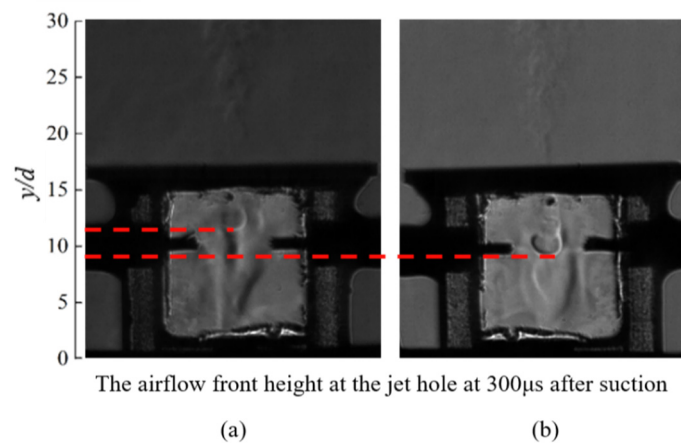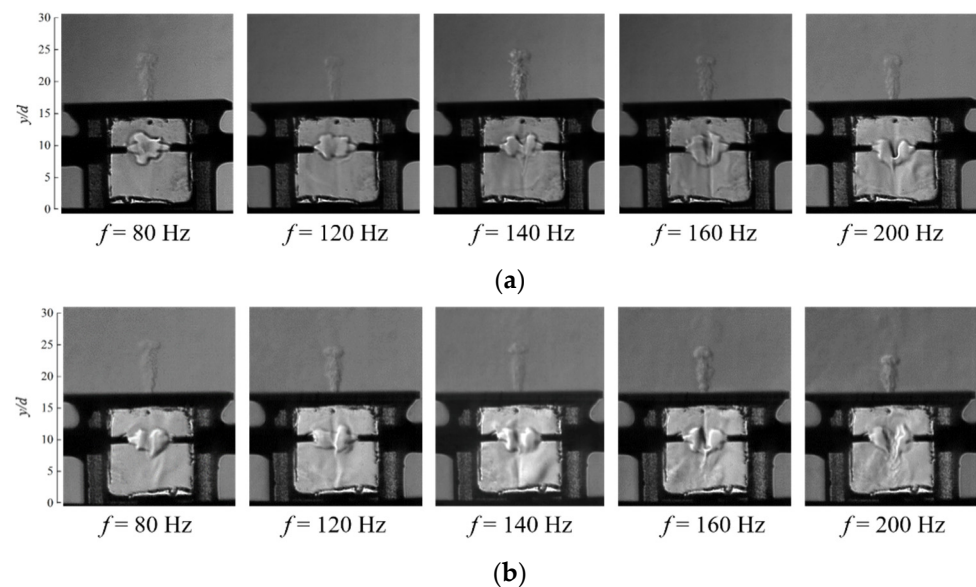

Figure 15. Comparison of the suction airflow front of the jet orifice at *f* = 200 Hz: (**a**) conventional excitation; (**b**) air supplement excitation.

Figure 16. Curves of inspiratory airflow parameters of the jet orifice with time at *f* = 200 Hz: (**a**) dimensionless height; (**b**) velocity.

The core of the heat source reflects the heating effect of discharge energy on the gas in the cavity. When the actuator operated continuously in the effective frequency band, the heat source core produced a clear depression during an expansion (Figures 12 and 13). This depression occurred in the upper part of the heat source core, thus inhibiting the normal upward expansion of the heat source core. This, in turn, affected the production of the jet and reduced the jet's velocity. The depression gradually increased with the expansion of heat source core, and continuous development caused the heat source core to completely separate along the depression.

A transverse comparison of schlieren images in the cavity under different frequencies and working conditions at $t = 400$ μs, as shown in Figure 17, was performed to observe the difference in the influence of the heat source core on the depression. Evidently, when the working frequency was the same, the influence of the depression on the expansion process of the heat source core under air supplement excitation was weaker than that under conventional excitation. In addition, the initial frequency (140 Hz) of the heat source core defects in the air supplement excitation state was higher than that in the conventional excitation state (120 Hz). In general, with an increase in the working frequency of the actuator, the heat source core was significantly affected by the depression.


$f = 80$ Hz $f = 120$ Hz $f = 140$ Hz $f = 160$ Hz $f = 200$ Hz

(**a**)

$f = 80$ Hz $f = 120$ Hz $f = 140$ Hz $f = 160$ Hz $f = 200$ Hz

(**b**)

Figure 17. Comparison of the flow field in the cavity at $t = 400$ μs under different excitation: (**a**) air-supplied excitation; (**b**) conventional excitation.

The reason for this phenomenon is that when the actuator operates in the effective frequency band, the discharge frequency is high (hundreds of hertz), and the inspiratory recovery process of the previous working cycle is not yet complete before entering the next working cycle for discharge. At the beginning of the next working cycle, an external atmosphere is sucked into the discharge cavity from the jet hole. The movement of the airflow in the discharge cavity is observed in the schlieren image (Figure 13), thus indicating that the gas density distribution in the discharge cavity is not uniform. When discharging in the next working cycle, the uneven distribution of air in the cavity expands at different speeds, thus leading to a hollow heat source core. Moreover, the higher the frequency of the actuator, the shorter the duration of the inspiratory recovery phase, the less sufficient the suction of the discharge cavity before the next working cycle, the more uneven the gas density, and the more evident the heat source core depression. Owing to the presence of the one-way valve, the inspiratory recovery speed is improved, which enhances the uniformity of the gas density distribution in the chamber and slows down the effect of the heat source depression, thus increasing the jet speed.

The expansion process of the heat source core observed in this experiment is similar to that observed by Shi et al. [25]; however, no heat source core depression has been reported in the literature. This is because the discharge frequency of the actuator used in this study was 1 Hz, and the inspiratory recovery process was complete. In this experiment, the discharge frequency reached tens or even hundreds of hertz, the working cycle was short, and the inspiratory recovery duration was small. In addition, owing to the different volumes and structures of the actuator, the shape development of the heat source core was different.

4. Inner Flow Model of Air-Supplied Plasma Synthetic Jet Actuator

Based on the flow evolution process in the cavity of the actuator obtained from the abovementioned invalid and effective working frequency bands, the internal working mechanism of the air-supplied PSJA was clarified, and the working mechanism models of the actuator at different working frequency bands were determined, as shown in Figures 18 and 19.
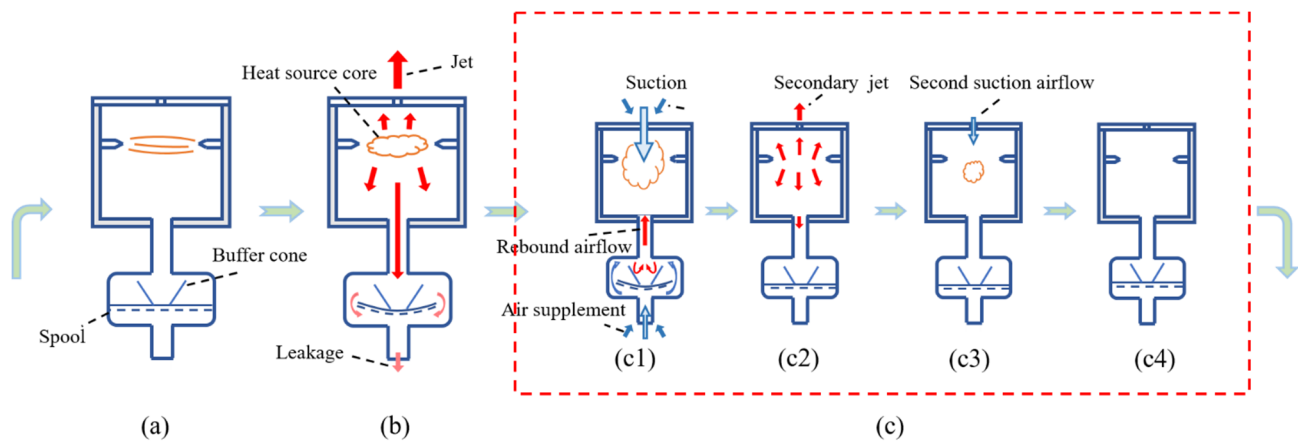
Figure 18. Inner flow model of the air-supplied actuator in the invalid frequency band: (**a**) spark discharge; (**b**) jet ejection; (**c**) inspiratory recovery: (**c1**) first suction (**c2**) secondary jet (**c3**) secondary suction airflow (**c4**) return to initial state.
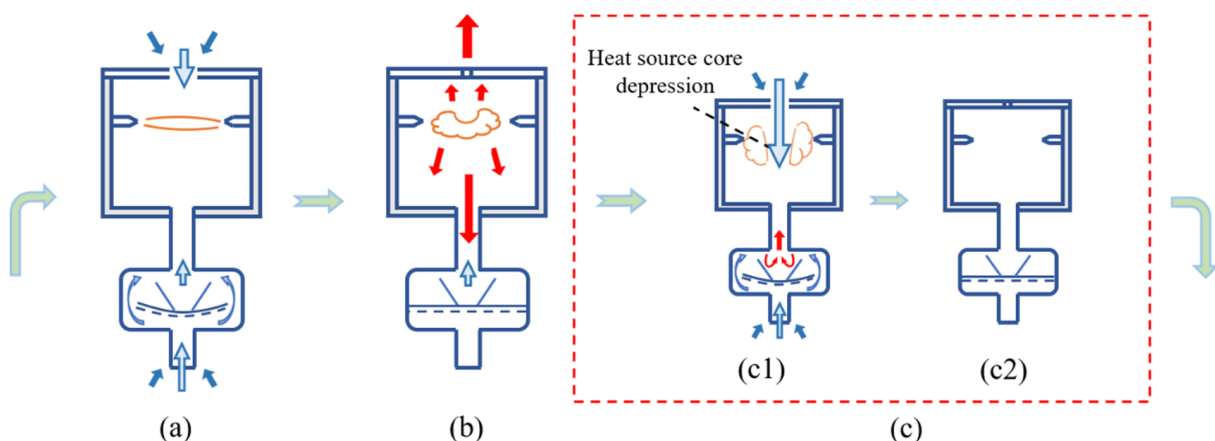
Figure 19. Inner flow model of the air-supplied actuator in the effective frequency band: (**a**) spark discharge; (**b**) jet ejection; (**c**) inspiratory recovery: (**c1**) first suction (**c2**) return to initial state.

4.1. Invalid Working Frequency Band

In the discharge stage, for the invalid working frequency band, the pressure in the cavity was higher, the breakdown voltage was higher, and the spark discharge deposited

additional energy. In the jet ejection stage, the core of the heat source generated by the discharge expanded, thus causing the air in the upper part of the cavity to be ejected via the jet hole to form a jet, and the lower part of the gas enters the one-way valve. The spool film of the one-way valve was deformed owing to the impact of the high-pressure gas, thus resulting in slight air leakage, as shown in Figure 18b. Therefore, the jet velocity was affected and reduced. In the inspiratory recovery stage, the discharge cavity became a low-pressure area after the jet was completely ejected. Under the action of the pressure difference, the actuator inhaled via the jet hole, and concurrently, the gas rapidly moved into the one-way valve in the jet ejection stage for rebound. Subsequently, the one-way valve was recharged to jointly fill the gas in the discharge cavity, as shown in Figure 18(c1). Owing to the inertia of the inspiratory airflow and the drop in cavity temperature, the pressure in the cavity was greater than the ambient pressure. Driven by the internal and external pressure differences, a secondary jet was formed, as shown in Figure 18(c2). After the end of the secondary jet flow, the pressure in the cavity was lower than the ambient pressure. Under the action of negative pressure, external air is inhaled into the cavity, thus resulting in secondary inspiration. However, the internal and external pressure differences were small at this time, and the inspiratory air generated was weak (Figure 18(c3)). Finally, the state of the gas in the cavity returned to the initial level and was prepared for discharge in the next cycle, as shown in Figure 18(c4), thus forming a complete working cycle of the air-replenishment type actuator.

4.2. Effective Working Frequency Band

For the effective working frequency band in the discharge stage, the inspiratory recovery of the actuator in the air supplement excitation state was fuller, the pressure in the cavity and breakdown voltage were higher, and the spark discharge energy and deposition energy were larger (Figure 19a). In the ejection stage, the core of the heat source generated by the discharge expanded, and the inner pressure increased abruptly. Under the action of the pressure difference, the air in the upper part of the cavity was ejected via the jet hole to generate a high-velocity jet. Compared with the conventional excitation state, additional energy was deposited in the charging stage under the air replenishment state; thus, the jet velocity was higher. Simultaneously, the gas entered the one-way valve, and the high-pressure airflow met the replenishment air flow of the one-way valve to be buffered, as shown in Figure 19b. In addition, owing to the insufficient mixing of gas in the cavity and uneven distribution of the gas density in the cavity during high-frequency operation, defects were formed in the core of the heat source and gradually developed, as shown in Figure 19b,c. Air replenishment using the one-way valve can effectively alleviate the influence of the sag on the expansion process of the core of the heat source and is conducive to the improvement of jet velocity. Under the action of negative pressure, the actuator was suctioned via the jet hole. Simultaneously, the buffered gas in the one-way valve returned, and the one-way valve performed additional air replenishment to jointly fill the gas in the discharge cavity. The inspiratory airflow rate of the actuator from the jet hole was significantly higher. Coupled with the extra air replenishment of the one-way valve, the inspiratory recovery of the discharge cavity was complete, and only one inhalation was required to complete the recovery. The pressure in the cavity was closer to the initial discharge state, thus providing adequate preparation for energy deposition in the discharge stage (Figure 19c). The abovementioned processes constitute to the working cycle of the air replenishment actuator in the effective acting frequency band.

5. Conclusions

(1) The peak current and voltage of the air-replenishing actuator in the ineffective frequency band did not increase significantly during spark discharge, the discharge energy remained unchanged within a single cycle, and the efflux performance did not improve.

(2)　The air supplement excitation state actuator could recover the air pressure state in the cavity more rapidly. The phenomenon of multiple jet hole replenishments in the conventional excitation state was avoided.

(3)　In the effective frequency band, the peak voltage and current during spark discharge were improved to a certain extent, and the discharge energy within a single cycle increased by 18.9%.

(4)　In the effective frequency band, the suction airflow velocity increased exponentially in the inspiratory recovery stage. Only one suction was required to complete the recovery process, and inspiratory recovery enhanced the uniformity of the gas density distribution in the cavity.

(5)　The air replenishment effect of the one-way valve alleviated the influence of the core sag of the heat source on its expansion, which increased both the negative pressure required for jet generation and jet energy generation.

(6)　For future work, a transparent air replenishment one-way valve can be developed to study the flow state inside the one-way valve and improve its structure of the one-way valve.

Author Contributions: Conceptualization, R.L.; methodology, W.W.; investigation, W.W.; writing—original draft preparation, R.L., W.W. and S.X.; writing–review and editing, R.L. and S.X.; project administration, Q.L.; funding acquisition, K.T. All authors have read and agreed to the published version of the manuscript.

Data Availability Statement: Not applicable.

Conflicts of Interest: The authors declare no conflict of interest.

References

1. Ikhlaq, M.; Yasir, M.; Demiroğlu, M.; Arik, M. Synthetic Jet Cooling Technology for Electronics Thermal Management—A Critical Review. *IEEE Trans. Compon. Packag. Manuf. Technol.* **2021**, *11*, 1156–1170. [CrossRef]
2. Grossman, K.R.; Cybyk, B.Z.; VanWie, D.M. Sparkjet actuators for flow control. In Proceedings of the 41st AIAA Aerospace Sciences Meeting and Exhibit, Reno, NV, USA, 6–9 January 2003; pp. 1–9.
3. Cybyk, B.Z.; Simon, D.H.; Land, H.B., III. Experimental characterization of a supersonic flow control actuator. In Proceedings of the 44th AIAA Aerospace Sciences Meeting and Exhibit, Reno, NV, USA, 9–12 January 2006; pp. 1–12.
4. Sarah, J.H.; Bruce, L.H.; Cybyk, B.Z.; Ko, H.; Katz, J. Characterization of a high-speed flow control actuator using digital speckle tomography and PIV. In Proceedings of the 4th Flow Control Conference, Seattle, WA, USA, 23–26 June 2008; pp. 1–12.
5. Popkin, S.H.; Cybyk, B.Z.; Land, H.B., III; Foster, C.; Emerick, T.; Alvi, F. Recent performance-based advances in Sparkjet actuator design for supersonic flow applications. In Proceedings of the 51st AIAA Aerospace Sciences Meeting Including the New Horizons Forum and Aerospace Exposition, Grapevine, TX, USA, 7–10 January 2013; pp. 1–11.
6. Popkin, S.H.; Cybyk, B.Z.; Foster, C.H.; Alvi, F.S. Experimental estimation of Sparkjet efficiency. *AIAA J.* **2016**, *54*, 1831–1845. [CrossRef]
7. Zong, H.H.; Pelt, V.T.; Kotsonis, M. Airfoil flow separation control with plasma synthetic jets at moderate Reynolds number. *Exp. Fluids* **2018**, *59*, 169. [CrossRef]
8. Sun, J.; Niu, Z.G.; Liu, R.B.; Liu, Q. The wind tunnel test of the active flow control on the flying wing model based on the plasma synthetic jet. *J. Exp. Fluid Mech.* **2019**, *33*, 81–88.
9. Chedevergne, F.; Léon, O.; Bodoc, V.; Caruana, D. Experimental and numerical response of a high-Reynolds-number M = 0.6 jet to a plasma synthetic jet actuator. *Int. J. Heat Fluid Flow* **2015**, *56*, 1–15. [CrossRef]
10. Emerick, T.; Ali, M.Y.; Foster, C.; Alvi, F.S.; Popkin, S. SparkJet characterizations in quiescent and supersonic flowfields. *Exp. Fluids* **2014**, *55*, 1858. [CrossRef]
11. Zhou, Y.; Xia, Z.X.; Luo, Z.B.; Wang, L.; Deng, X.; Zhang, Q.; Yang, S. Characterization of three-electrode sparkjet actuator for hypersonic flow control. *AIAA J.* **2018**, *57*, 879–885. [CrossRef]

12. Wang, H.Y.; Li, J.; Jin, D.; Tang, M.; Wu, Y.; Xiao, L. High-frequency counter-flow plasma synthetic jet actuator and its application in suppression of supersonic flow separation. *Acta Astronaut.* **2018**, *142*, 45–56. [CrossRef]

13. Tang, M.X.; Wu, Y.; Wang, H.Y.; Shanguang, G.; Zhengzhong, S.; Jiaming, S. Characterization of transverse plasma jet and its effects on ramp induced separation. *Exp. Therm. Fluid Sci.* **2018**, *99*, 584–594.

14. Gu, R.Y.; Shan, Y.; Zhang, J.Z. Numerical study on transport aircraft after-body flow separation control by spark jet. *J. Aerosp. Power* **2018**, *33*, 1855–1863.

15. Liu, R.B.; Wei, W.T.; Li, F.; Lin, Q. Working mechanism of air-supplemented plasma synthetic jet actuator. *Acta Aeronaut. Astronaut. Sin.* **2022**, *43*, 125854-1–125854-15.

16. Wang, L.; Luo, Z.B.; Xia, Z.X.; Liu, B.; Deng, X. Review of actuators for high speed active flow control. *Sci. China Tech. Sci.* **2012**, *55*, 2225–2240. [CrossRef]

17. Zhou, Y.; Luo, Z.B.; Wang, L.; Xia, Z.X.; Gao, T.X.; Xie, W.; Deng, X.; Peng, W.Q.; Cheng, P. Plasma synthetic jet actuator for flow control: Review. *Acta Aeronaut. Astronaut. Sin.* **2022**, *43*, 98–140.

18. Zhou, Y.; Xia, Z.X.; Luo, Z.B.; Wang, L.; Deng, X. A novel ram-air plasma synthetic jet actuator for near space high-speed flow control. *Acta Astronaut.* **2017**, *133*, 95–102. [CrossRef]

19. Li, J.F.; Zhang, X.B. Active flow control for supersonic aircraft: A novel hybrid synthetic jet actuator. *Sens. Actuators A Phys.* **2020**, *302*, 111770. [CrossRef]

20. Emerick, T.M.; Ali, M.Y.; Foster, C.H.; Alvi, F.; Haack Popkin, S.; Cybyk, B. Sparkjet actuator Characterization in supersonic crossflow. In Proceedings of the 6th AIAA Flow Control Conference, New Orleans, LA, USA, 25–28 June 2012; pp. 1–10.

21. Zhou, Y.; Xia, Z.X.; Luo, Z.B.; Zhou, Y.; Liu, Q.; Peng, W. Characterization of plasma synthetic jet actuator with cavity pressurization. *J. Natl. Univ. Def. Technol.* **2019**, *41*, 12–18.

22. Zong, H.H.; Liang, H.; Song, G.Z. Self-Air-Supplementing Type Double-Cavity Plasma Synthetic Jet Actuator. CN 113993266 A, 28 January 2022.

23. Zheng, B.R.; Zhang, Q.; Zhao, T.F.; Song, G.; Chen, Q. Experimental and numerical investigation of a self-supplementing dual-cavity plasma synthetic jet actuator. *Plasma Sci. Technol.* **2023**, *25*, 025503. [CrossRef]

24. Liu, R.B.; Wang, M.M.; Hao, M.; Lin, Q.; Wang, X.G. Experimental research on air supplementing type plasma synthetic jet generator. *Acta Aeronaut. Astronaut. Sin.* **2016**, *37*, 1713–1721.

25. Dong, H.; Geng, X.; Shi, Z.W.; Cheng, K.; Cui, Y.D.; Khoo, B.C. On evolution of flow structures induced by nanosecond pulse discharge inside a plasma synthetic jet actuator. *Jpn. J. Appl. Phys.* **2019**, *58*, 028002-1–028002-5. [CrossRef]

26. Li, F. *Study on Improving the Performance and Working Mechanism of Plasma Synthetic Jet Actuator by Check Valve*; Xiamen University: Xiamen, China, 2020.

27. Liu, R.B.; Li, F.; Wei, W.T.; Chen, G.T.; Lin, Q. One-Way Valve and Plasma Synthetic Jet Actuator. 2021. Available online: https://kns.cnki.net/kcms2/article/abstract?v=3uoqIhG8C475KOm_zrgu4sq25HxUBNNTmIbFx6y0bOQ0cH_CuEtpsJF6UDXkM2RHxcfw9n9uIkLTMRp6TRxTKpw8R11ferAG&uniplatform=NZKPT (accessed on 28 January 2023).

28. Liu, R.B.; Lin, R.X.; Lian, G.C.; Xue, S.; Lin, Q. Multichannel plasma synthetic jet actuator driven by Marx high-voltage generator. *AIAA J.* **2021**, *59*, 3417–3430. [CrossRef]

29. Zong, H.; Kotsonis, M. Formation, evolution and scaling of plasma synthetic jets. *J. Fluid Mech.* **2018**, *837*, 147–181. [CrossRef]